ELSEVIER

Materials Science and Engineering A285 (2000) 99–110

MATERIALS SCIENCE & ENGINEERING A

www.elsevier.com/locate/msea

Effects of dispersed microvoids on thermal expansion behavior of composite materials

Hiroshi Hatta [a,*], Takako Takei [b], Minoru Taya [c]

[a] *The Institute of Space and Astronautical Science, 3-1-1 Yoshinodai, Sagamihara-Shi, Kanagawa-Ken 229, Japan*
[b] *Materials and Electronic Devices Laboratory, Mitstubishi Electric Corporation, 1-1-57 Miyashimo, Sagamihara-Shi, Kanagawa-Ken 229, Japan*
[c] *Department of Mechanical Engineering, University of Washington, Seattle, WA 98195, USA*

Abstract

In our earlier papers [T. Takei, H. Hatta, M. Taya, Mater. Sci. Eng. A131 (1991) 133; T. Takei, H. Hatta, M. Taya, Mater. Sci. Eng. A131 (1991) 145], we found that the coefficients of thermal expansion (CTEs) of particulate composites are lowered by dispersed microvoids in the matrix. In order to prove this void dispersion effect by an analytical model and to utilize this effect for wide control of composite CTE, an analytical parametric study is conducted in this paper. It is found in this study that the combination of fiber type reinforcement with high elastic modulus and low CTE and disk-shaped voids was identified to remarkably lower the composite CTE. This CTE control technique is based on the mechanism that microvoids in the matrix are compressed by compressive stress field developed around reinforcement when the composite is subjected to temperature rise. In order to confirm experimentally this void dispersion effect on CTEs, three types of composite materials with dispersed voids in their matrices were fabricated, particulate, short fiber, continuous fiber (3D) reinforced composites, and CTEs of these composites were measured. It was concluded from comparison between the predictions and experimentally observed CTEs that the CTE reduction by the void dispersion actually occurs and this effect is analytically predictable up to some limit volume fraction, which depends on a composite type.

1. Introduction

One of significant features of a composite material is tailorability of its material properties. Coefficient of thermal expansion (CTE) of a composite material is known to play a key role, for instance, in designing electronic packaging materials such as an IC board where the CTE of the board is desired to be as close as that of a silicon substrate. Since most of electronic packaging materials are made of polymer or polymeric composites and the CTE of a polymer is high, we made some efforts to lower the CTEs of an IC board made of a polymeric composite by controlling the volume fraction and shape of fillers with smaller CTEs. It was found in the previous studies that there exists an upper limit on volume fraction of fillers (V_f) due to difficulty in processing although increasing V_f is known to lower the CTE of a polymeric composite. The main difficulty in processing a polymeric composite with higher V_f is inclusion of voids, which were formed during processing. We found in our earlier studies that the CTE of a composite was reduced by the existence of voids in the matrix. This effect of voids on lowering composite CTE was also observed by Fujimoto and Noda [3].

Noda and Fujimoto [3] fabricated a particulate composite with low elastic modulus and CTE in an attempt to develop an electronic packaging material. Their composite consisted of silica particle, silicon rubber particle, and epoxy resin. The silicon rubber particles in this composite are expected to play the role of microvoids. Since the CTE of the silicon rubber is about 3×10^{-4}, approximately five times larger than that of the matrix resin (6×10^{-5}), the debonding of the interface, between the matrix/silicon rubber particles occurred during cooling down process from curing temperature (120°C) to room temperature due to large amount shrinkage of the silicon rubber particles as shown in Fig. 1. In this figure, a, b, and c denote schematically the silica particles and silicon rubber particles in a composite, the composite with voids converted from silicon rubber particles, and actual fracture surface, for the matrix part of this composite, respectively. It is

* Corresponding author. Tel.: +42-759-8293; fax: +42-759-8461.

0921-5093/00/$ - see front matter
PII: S0921-5093(00)00721-8

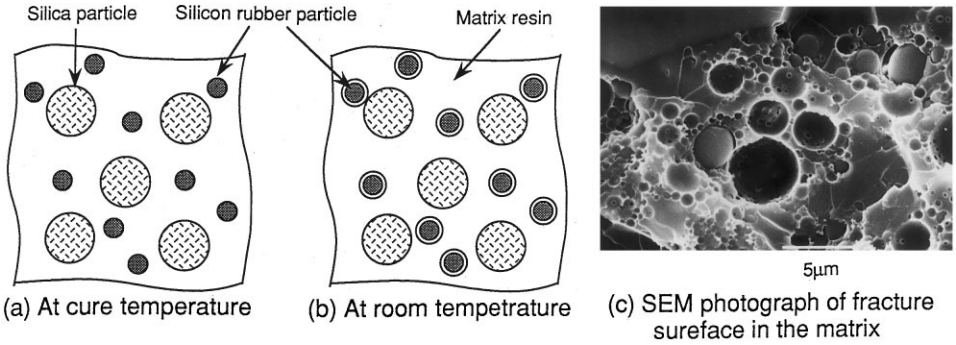

Fig. 1. Illustrative figures for formation of voids in the matrix in particulate filled composite (a), (b) and SEM microphotograph of a typical fracture surface of the composite (c).

obvious from Fig. 1c that the complete debonding and the resulting falling away of silicon rubber particles from the matrix during a fracture process of the composite are observed, supporting the hypothesis of Fig. 1b. Fig. 2 shows the measured CTE of the silica particle/epoxy composite, where open and filled circles stand for two cases, the volume fractions of the voids being nearly zero (void free) and about 12% (weight fraction of the silicon rubber particles $W_r = 10\%$), respectively, and the solid and dashed lines denote the corresponding theoretical predictions based on our model discussed later. It can be concluded from Fig. 2 that the composite CTE is remarkably reduced by the existence of the microvoids.

The above observations led us to write this paper with the aim to propose a new method to start control composite CTE by use of this void effect. First we shall state an analytical model for a composite with dispersed voids in Section 2. The results of a parametric study based on the present model to find out which parameters have dominant influence to reduce the composite CTE will be given in Section 3. In order to prove that the present model is effective in explaining the void effect on composite CTE reduction, we processed several composites with voids, particulate, short fiber and three dimensional (3D) continuous fiber composites. The processing route of these composites are given in Section 4, followed by discussion in Section 5, where comparisons between the present model and the CTEs of the composites with voids processed by other researchers and by us, are made. Finally concluding remarks are stated in Section 6.

2. Analytical modeling

In this analytical study, we will use three types of analytical models, (1) Eshelby's model [4] modified for finite volume fraction of fillers; (2) thinly coated model; and (3) void dispersion model. The first is applied to particulate and short fiber composites with voids while the second and third types to 3D continuous fiber composite with voids.

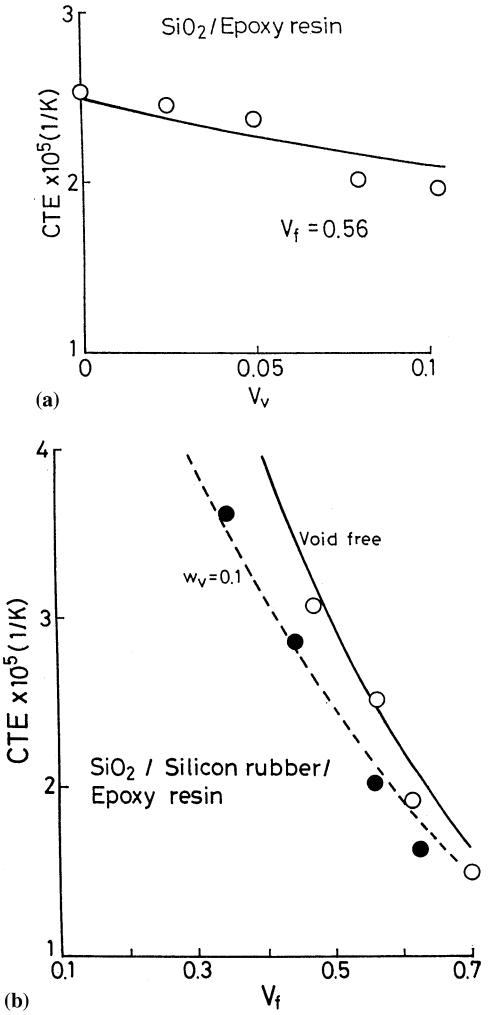

Fig. 2. CTE of the particulate composite as a function of void volume fraction V_v, (a) and filler volume fraction V_f, (b).

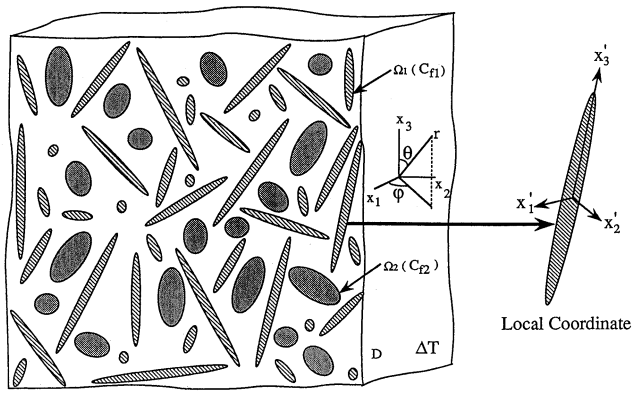

Fig. 3. An analytical model to calculate CTE of a short fiber composite with dispersed voids.

2.1. Eshelby's model

Many analytical models have been proposed to predict CTE of a composite. Analytical models proposed before 1975 were reviewed by Hale [5]. After that various extensions to deal with complex material systems were conducted including effect of plasticity in the matrix [6,7], multi-reinforcing phases [8], interaction effect of temperature and moisture [9], and effect of reinforcement misorientation [10,11]. Among analytical models to predict CTE of a composite material, the Eshelby's equivalent inclusion method modified for finite volume fraction of filler, Takao and Taya [12] and Takao [11], is most flexible and convenient to simulate a complex microstructure of a material system. Thus, in this paper we extend the Takao's model to the case of a composite with microvoids.

The analytical model is shown in Fig. 3, where two kinds of reinforcement is dispersed 3D-randomly in the matrix and the whole composite body D is subjected to uniform temperature difference ΔT. The ellipsoids with different aspect ratios in this figure are to manifest 3D-random orientation of reinforcements. In the derivation of the composite CTE, Takao [11] considered general case of N kinds of reinforcement dispersed in the matrix, instead of two kinds of reinforcement in the figure, and obtained the following expression for the CTEs of the hybrid composite

$$\alpha_c = \alpha_m - \frac{1}{V_D}\sum_{i=1}^{N}\int_{\omega_i} f_i \left\{ \int_{\Omega_\tau} \boldsymbol{T}_c \cdot \boldsymbol{G}_{1i} \cdot \boldsymbol{T}_c^{-1}\, d\Omega_i \cdot \dot{\boldsymbol{e}} + \int_{\Omega_i} \boldsymbol{T}_c \cdot \boldsymbol{G}_{2i} \cdot \boldsymbol{\alpha}_i^{*\prime}\, d\Omega \right\} d\omega_i \quad (1)$$

In Eq. (1), the bold face letters represent tensorial quantities, the dot stands for the inner product between tensorial quantities, and $\boldsymbol{\alpha}_i^*$ denotes the thermal mismatch strain tensor defined by

$$\boldsymbol{\alpha}_i^* = \alpha_{fi} - \alpha_m \quad (2)$$

where α_{fi} and α_m are the CTEs of the ith filler and matrix α_m. V_D, f_i, ω_i, Ω_i and $\mathbf{T}_c$ in Eq. (1) denote the volume of the entire composite, orientation distribution density of the ith reinforcing phase, area in the orientation distribution space (might be on unit sphere), the domain of the ith reinforcing phase, and coordinate transformation tensor from local to global coordinate, respectively. The local and global coordinates, designated by $x,'$ and $x,,$ are defined as shown in Fig. 3 and quantities referred to the local coordinate are expressed by superscript prime. Note that in the local coordinate system associated with reinforcement, the x'_3 axis coincides with the axial direction of the reinforcement. $\boldsymbol{G}_{1i}$ and $\boldsymbol{G}_{2i}$ in Eq. (1) are the fourth order tensor defined by

$$\boldsymbol{G}'_{1i} = \{(\boldsymbol{C}'_{fi} - \boldsymbol{C}'_{mi}) \cdot (\boldsymbol{S}'_i - \boldsymbol{I}) + \boldsymbol{C}'_{fi}\}^{-1} \cdot (\boldsymbol{C}'_{fi} - \boldsymbol{C}'_{mi})$$
$$\boldsymbol{G}'_{2i} = \{(\boldsymbol{C}'_{fi} - \boldsymbol{C}'_{mi}) \cdot (\boldsymbol{S}'_i - \boldsymbol{I}) + \boldsymbol{C}'_{fi}\}^{-1} \cdot \boldsymbol{C}'_{fi} \quad (3)$$

where $\boldsymbol{C}_{fi}$, $\boldsymbol{C}_{mi}$, $\boldsymbol{I}$, and $\boldsymbol{S}_i$, denote the elastic stiffness tensor of the ith reinforcement and the matrix, the identity tensor, and the Eshelby tensor for the ith reinforcement and superscript -1 denotes the inverse of the fourth order tensors. The Eshelby tensor [4] is a function of the matrix Poisson's ratio and the shape of the reinforcements. $\dot{\boldsymbol{e}}$ in Eq. (1) is the average strain in the matrix and can be obtained by solving the following simultaneous equation.

$$\boldsymbol{I} - \frac{1}{V_D}\sum_{i=1}^{N}\int_{\omega_i} f_i \left\{ \int_{\Omega_i} \boldsymbol{T}_c \cdot (\boldsymbol{S}'_i - \boldsymbol{I}) \boldsymbol{G}_{1i} \cdot \boldsymbol{T}_c^{-1}\, dV_i\, d\omega_i \right\} \cdot \dot{\boldsymbol{e}} = \frac{1}{V_D}\sum_{i=1}^{N}\int_{\omega_i} f_i \left\{ \int_{\Omega_i} \boldsymbol{T}_c \cdot (\boldsymbol{S}'_i - \boldsymbol{I}) \boldsymbol{G}_{2i} \cdot \boldsymbol{\alpha}_i^{*\prime}\, dV \right\} d\omega_i \quad (4)$$

When the orientation distribution f_i, is assumed to be axisymmetric about the x_3 axis, hence independent of angle ϕ. Volume element, $d\omega_i = \rho_i(\theta) \sin\theta\, d\theta\, d\phi$. A substitution of $d\omega_i$ into Eq. (1) yields the solution to α_c for a 3D axisymmetric orientation distribution. For the case of aligned fillers and voids Eq. (1) reduces to

$$\alpha_c = \alpha_m - \sum_{i=1}^{N} V_{fi}(\boldsymbol{G}_{1i} \cdot \dot{\boldsymbol{e}} - \boldsymbol{G}_{2i} \cdot \boldsymbol{\alpha}_i^{*\prime}) \quad (5)$$

2.2. Analytical model for a 3D composite

The above-mentioned analytical model to predict CTEs of composite materials with dispersed microvoids is directly applicable to short fiber and carbon/carbon composites. On the other hand, for void-dispersed (skeletonized) 3D composites, two kinds of analytical models illustrated in Fig. 4 were developed [13]. The void-dispersion model for a 3D composite is a combination of the void-dispersion model and the 3D composite model [15]. This model assumes that the voids in a composite are uniformly dispersed in the matrix as illustrated in Fig. 4b. On the other hand, actual voids in

the skeletonized 3D composite are located at the center of unit cell, (see Fig. 14e). Thus this model is effective only when the volume fraction of the voids V_v, is low, because this model neglects the effect of relative locations of the reinforcing rods and voids.

The second model is thinly coated rod model shown in Fig. 4a. In this model, CTEs were calculated based on the assumption that the CTEs of the skeletonized 3D composites coincide with the axial CTE of the resin-coated CFRP rods in which the dipping (matrix) resin is equally divided into individual reinforcing axes. This model predicts precise values only in the limiting case of the, high void volume fraction, i.e. volume fraction of dipping resin is very low. Actually, the resin applied in the dipping process takes meniscus form at around contact point of the rods as shown in Fig. 14e.

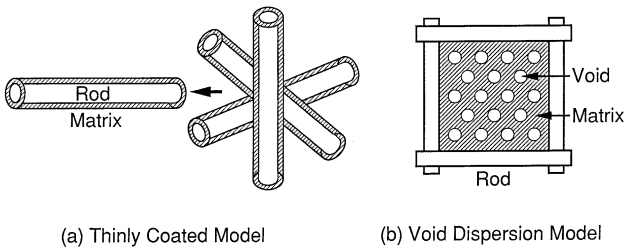

Fig. 4. Analytical models to simulate the thermal expansion behavior of the skeletonized composites, (a) thinly coated model; (b) void dispersion model.

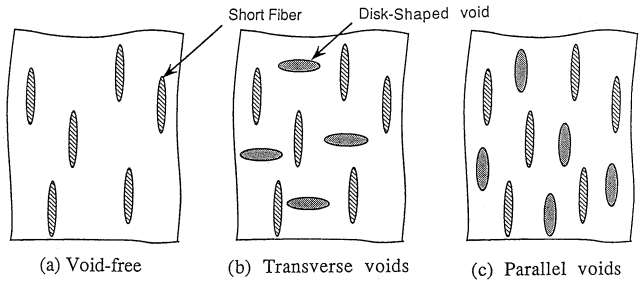

Fig. 5. Schematic diagram to explain orientation of the microvoids dispersed in the matrix.

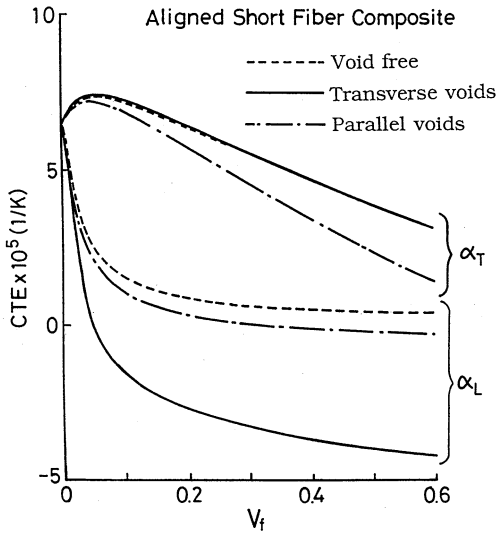

Fig. 6. Effect of void orientation on CTE of an aligned short fiber composite.

3. Parametric study

For a parametric study, the first reinforcement in Eq. (1) is set equal to real reinforcement (mainly short fiber) and second one to void whose elastic modulus and CTE are set equal to zero. Only the combination of three cases of orientation distribution of the reinforcement and void is considered; unidirectionally aligned, 2D random, and 3D random, because these cases are most important in actual composites. In the computation, the following data for constituents, which simulate a polymer matrix composite with ceramic short fibers, are used.

Ceramic fiber, $E_f = 385$ GPa, $\nu_f = 0.27$, $\alpha_f = 2 \times 10^{-6}$ K^{-1}, $As_f = 17.5$, $V_t = 0.3$

Void, $E_v = 0$, $\alpha_v = 0$, $As_v = 0.1$ (disk-shaped), $V_v = 0.05$

Matrix, $E_m = 3.5$ GPa, $\nu_m = 0.38$, $\alpha_m = 6.8 \times 10^{-6}$ K^{-1}

where E, ν, α, As, and V denote the Young's modulus, Poisson's ratio, CTE, aspect ratio, and volume fraction, respectively, and subscripts f, v, and m represent the short fiber, void, and matrix phases, respectively. It is noted here that the representative shape of voids is assumed to be disk-shaped and all the constituents are assumed to be isotropic to simplify the calculations. In order to examine the effect of a parameter on the composite CTE, we changed one of a parameter while keeping the others unchanged (i.e. set equal to the above values).

3.1. Effect of shape and orientation of voids

Among various parameters, we shall examine first the effect of void orientation on CTE of a short fiber composite. The void orientation is defined in Fig. 5 where three cases of relative orientation of the fiber and voids are given, (a) void free; (b) the planes of disk-shaped voids are oriented transversely to the fiber axis (transverse voids); and (c) those of disk-shaped void parallel to the fiber-axis (parallel voids). The results of the CTEs of an aligned short fiber composite with three cases of void orientation predicted by the present model are shown in Fig. 4, where α_L and α_T represent the CTEs along the directions parallel and normal to the fiber axis, respectively. It is obvious from Fig. 6 that the disk-shaped transverse voids reduce α_L greatly whereas the parallel voids have much less effect. Thus, in the

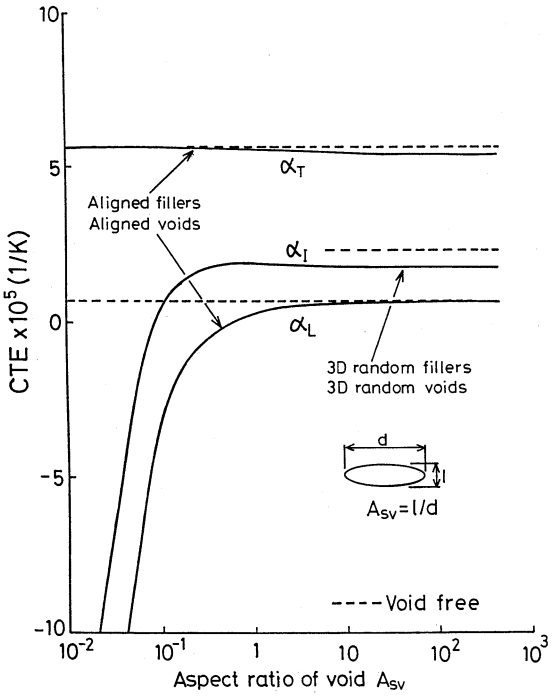

Fig. 7. Effect of aspect ratio of voids As_v on CTE of aligned and 3D random short fiber composites.

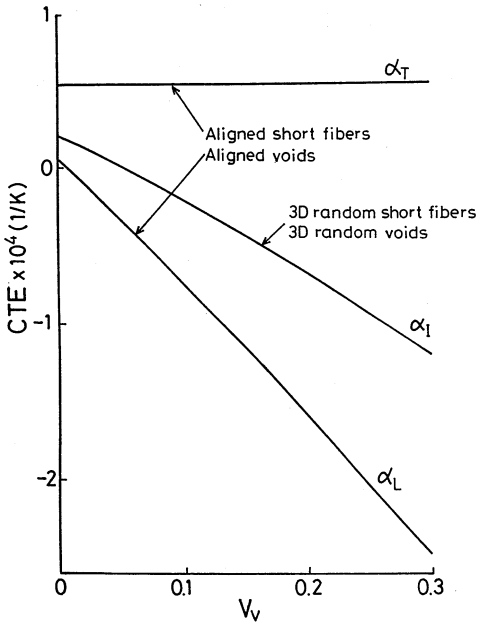

Fig. 8. Effect of volume fraction of voids V_v, on CTE of aligned and 3D random short fiber composites.

following, we shall mainly concentrate on the case of transverse disk-shaped voids (Fig. 5b). This strong effect of dispersed transverse voids is attributed to following reasons:

1. High magnitude of compressive stress due to CTE mismatch strain tends to be developed along the fiber-axis direction in an aligned short fiber composite.
2. The disk-shaped voids are easily forced to reduce its volume by the compressive stress along the void axis.

This effect of the transverse voids on α_L becomes enhanced for larger volume fraction of the short fiber. Thus, very low (even negative) values of CTE (-3 to -4×10^{-5}) can be obtained from the constituents with positive values of CTEs. These low values, however, may not be realized in actual composites, because, in the case of composite with low α_L, high magnitude of thermal stresses is induced in the matrix more likely to result in the fracture of the matrix–fiber interface. Thus, actually tailorable region of composite CTEs by introducing voids in the matrix may be narrower than this figure indicates.

Next we examine the effect of void shape (i.e. void aspect ratio, $As_v = 1/d$) on CTEs of two kinds of the short fiber composite (aligned and 3D random orientation). The analytical results are shown in Fig. 7 where the orientation of voids in an aligned composite is defined in Fig. 5b. It is noted in Fig. 7 that the macroscopic properties of a composite of 3D random orientation of voids are isotropic, including its CTE (α_I). The solid and dashed lines represent the cases of the composite with and without voids, respectively. Thus, the discrepancy between dashed and solid lines stands for the void effect. It follows from Fig. 5 that the void effect on composite CTEs becomes enhanced even for the composite with 3D random void orientation as well as the aligned short fiber composite especially when voids are disk-shaped, i.e. $As_v < 1$.

The effect of volume fraction of disk-shaped voids V_v, on the CTEs of composites with aligned and 3D random orientation voids is demonstrated in Fig. 8. Although composite CTEs decrease strongly with increase in V_v, the transverse CTE of a composite with aligned short fibers and voids (Fig. 5b) is insensitive to V_v.

Fig. 9 demonstrates the effect of Young's modulus (E_v) of dispersed soft spherical fillers on CTEs of shortfiber composite where the soft fillers can represent voids if E_v becomes zero and just the matrix material if E_v, becomes equal to the matrix Young's modulus; both cases are shown as open circles. It follows from the figure that the effect of soft particles with their elastic modulus over two orders of magnitude smaller than the matrix's modulus on reducing the composite, CTE is nearly the same as that of voids.

3.2. Effect of properties of reinforcement

In this section, let us examine the effects of reinforcement on the CTE, of a composite with disk-shaped voids. The effect of the Young's modulus of the reinforcement (short fibers) on composite CTE, is demon-

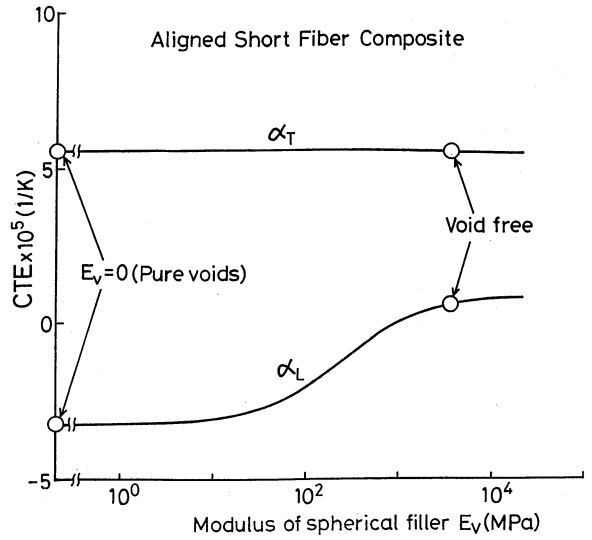

Fig. 9. Effect of modulus of spherical fillers dispersed in the matrix E_v on CTE of a short fiber composite.

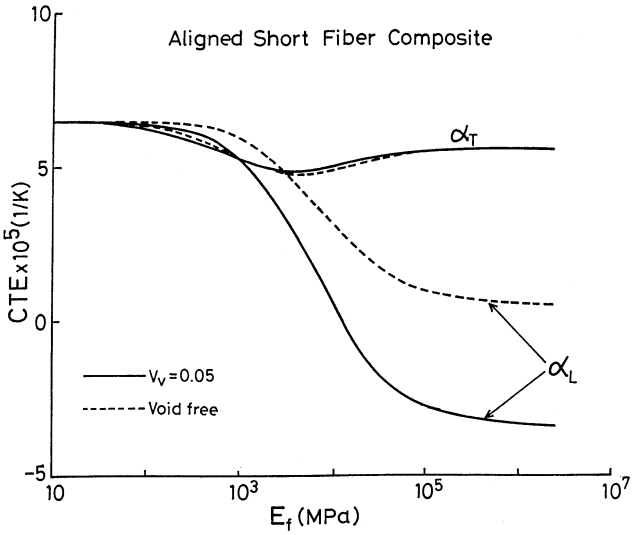

Fig. 10. Effect of fiber modulus E_f on CTE of aligned and 3D random short fiber composite.

strated in Fig 10 where α_L is seen to decrease due to the dispersed voids and this reduction in α_L increases with increase of the elastic modulus of the short fibers (E_f). This is because the compressive stress of higher magnitude can develop along the axis of the short fibers with higher values of E_f. By the same token, higher aspect ratio of short fiber As_f gives rise to higher magnitude of the compressive stress. Thus, α_L decreases with increase of As_f.

4. Experiment

In order to collect more evidence of the void effect on lowering composite CTE, we processed two different composites with voids, short fiber and 3D continuous fiber composite. The measurements of the CTEs are also made on the above composites as well as the laminated carbon/carbon composite specimens where all of them contain voids or cracks. Both processing and CTE measurement of the composites are discussed below. Constituent materials and material constants of these composites are listed in Tables 1–3.

4.1. Short fiber composite

The void-dispersed short fiber composites were fabricated by the processing route shown in Fig. 11. In this processing route, the Al_2O_3 short fiber and silicon rubber particles were at first formed into thick mat-like preform by conventional paper making process, the detailed process of which was given elsewhere [1,2]. After applying the coupling treatment to the preform, epoxy matrix was vacuum-infiltrated into the preform and then the resin-infiltrated preform was compression-molded at 120°C and 10 MPa for 2 h to cure the epoxy resin. This process gives rise to 2D-random distribution of Al_2O_3 short fiber. The silicon rubber particles in this composite are expected to play the role of microvoids. Void content V_v was varied by changing the volume fraction of the silicon rubber particles, while the volume fraction of short fiber in the composite, V_f, was made nearly a fixed value, about 20%, in order to elucidate the void effect.

4.2. 3D composites

Unidirectional carbon fiber reinforced plastics (CFRP) rods fabricated by the pultrusion process are manually assembled to fabricate tri-axially reinforced 3D preforms as shown in Fig. 12. The reinforcing rods

Table 1
Constituent materials of void-dispersed composites

Composites	Reinforcement	Void source	Matrix
Particulate composite	SiO_2 particle	Silicon rubber particles $d=5$ μm	Epoxy resin
Short fiber composite	2D random oriented Al_2O_3 short fiber	Silicon rubber particles $d=1.5$ μm	
Skeletonized 3D composite	Unidirectionally reinforcd CFRP	(Dipping process)	
Carbon/carbon composite	Carbon fiber Toray M461	Transverse cracks	Carbon

Table 2
Material properties used in calculations of fiber reinforced plastics

Composites	Reinforcement	Matrix	Void
Particulate composite	E, 70.0 GPa; ν, 0.22; α, 0.5×10^{-6} K^{-1}; As, 1; d, 1–5 μm	E, 3.5 GPa; ν, 0.35; α, $5–8\times10^{-5}$ K^{-1}	E, 0; ν, 0.22; α, 0
Short fiber composite	E, 300 GPa; ν, 0.22; α, 8×10^{-6} K^{-1}; As, 30	E, 3.4 GPa; ν, 0.38; α, 6.8×10^{-5} K^{-1}	
Skeletonized 3D composite	E_L:, 60 GPa; E_T, 10 GPa; G_{LT}, 5.3 GPa; ν_{LT}, 0.33; ν_{TL}, 0.0125; α_L, -8.7×10^{-7} K^{-1}; α_T, 5.0×10^{-5} K^{-1}	E, 3.5 GPa; ν, 0.38; α, 7.1×10^{-5} K^{-1}	

Table 3
Material properties used in calculation of carbon/carbon composite[a]

Temperature (°C)	20	250	500	750	1000	1250	1500
α_{fL} ($\times10^{-6}$/°C)	−1.33	−0.27	0.60	1.07	1.50	1.50	1.50
α_{mL} ($\times10^{-6}$/°C)	3.47	4.40	4.73	5.39	5.72	5.89	6.19
α_{mT} ($\times10^{-6}$/°C)	4.27	5.73	6.45	7.0	7.67	8.10	8.48

[a] α_{fT}, 6.0×10^{-5}; E_{fL}, 400 GPa; E_{fT}, 21 GPa; G_{LT}, 42 GPa; ν_{LT}, 0.31; ν_{TT}, 0.33; E_m, 20 GPa; ν_m, 0.3.

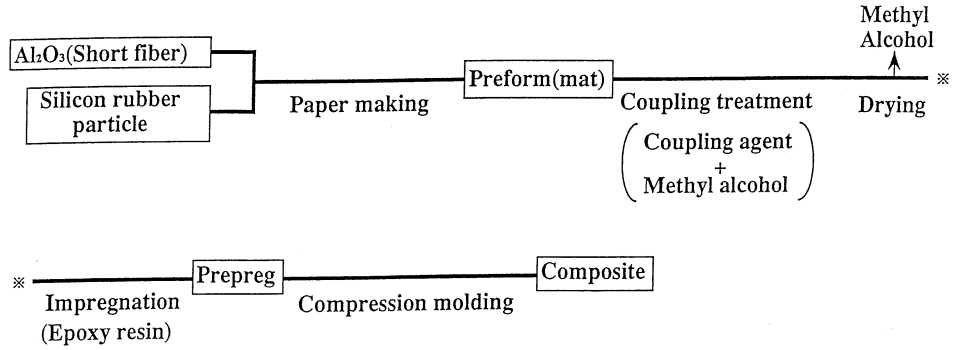

Fig. 11. Forming process of a short fiber composite by the combination of paper making and resin infiltration processes.

were made of Torayca N146J and epoxy resin and each rod has circular cross-section of diameter 0.68 mm. The rods are assembled as tightly as possible so as to maximize the volume fraction of the reinforcing rods (V_{rod}) in the preform. Thus, V_{rod} was about 58.9% in accordance with the theoretical value [14,15] and the volume fraction of the carbon fiber in the rod was 65%, resulting in the total volume fraction of the reinforcing fiber in the 3D composite being $58.9\times65\%=38\%$.

The assembled preforms were impregnated with matrix resin (epoxy) by dipping process to form skeletonized (porous) 3D composite as illustrated in Fig. 13, the detailed process of which was given elsewhere [13]. In this process, the preform was at first soaked in the varnish composed of epoxy resin and solvent, ethylene glycol monomethyl ether (Fig. 13a). Then the preform was taken out of the varnish and excess varnish was dripped off (Fig. 13b). Thus, the varnish was thinly coated on straight portion of rods and made into meniscus form in the vicinity of contact points of the reinforcing rods as shown in Fig. 13d. Finally the preform treated with the varnish was put in an oven to dry out the solvent and to cure the applied resin (Fig. 13e). The volume fraction of the dipping resin was

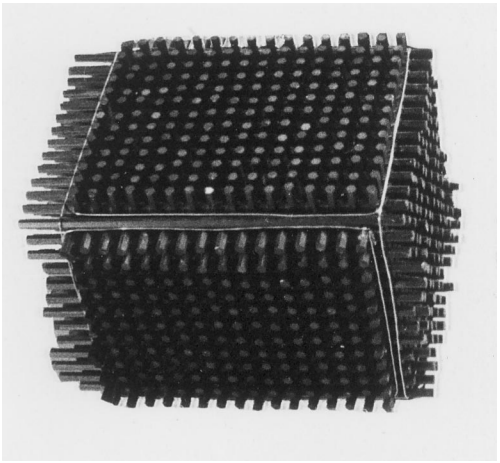

Fig. 12. Typical examples of the tri-axially reinforced 3D preforms made of unidirectionally reinforced CFRP rods.

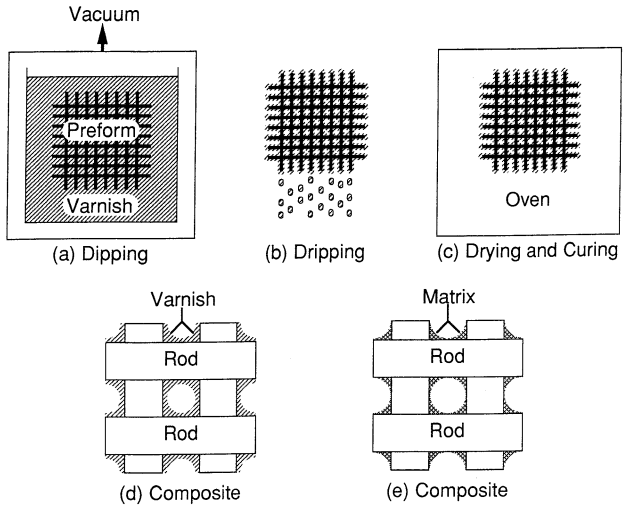

Fig. 13. Dipping process to apply the matrix resin to the 3D preform.

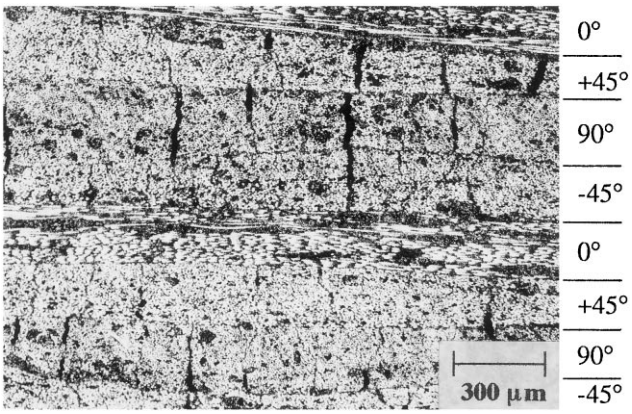

Fig. 14. Cross-sectional view of a quasi-isotropically laminated carbon/carbon composite.

varied by changing the concentration of the resin in the varnish and the repeating times of the dipping processes.

4.3. Carbon/carbon composite

Carbon/carbon composites of a laminate type often possess so-called 'transverse cracks', as typically shown in Fig. 14. The transverse cracks are induced due to the thermal expansion mismatch strain between the directions parallel and normal to the fiber axis. The carbon/carbon composites examined in this study were fabricated by so called 'preformed yarn method' [16] and were heat-treated at 2000°C. Hence a large amount of thermal expansion mismatch strain appeared during the cooling process to room temperature. Temperature range of CTE measurement of this composite was very wide, room temperature to 2000°C. Thus, temperature dependence of the material constants should be taken into account. The material constants used in the calculation are shown in Table 3, where temperature dependence of CTE values for carbon fiber and matrix carbon was estimated from the data of Yasuda [17], and Salto [19]. Only the laminate composite with quasi-isotropic stacking sequence was compared here.

4.4. Measurement of CTEs

For the short fiber and 3D composites, the samples used for CTE measurements were a rectangle of $8 \times 10 \times 20$ or 23 mm or a cube with 25 mm side length. A contact type thermo-mechanical analyzer (TMA) was used to measure CTE within the temperature range of -100 to 150°C and at the temperature increase rate of 2°C min^{-1}. The CTE measurements of the short fiber and 3D composites were conducted under continuous flow, 50 ml min^{-1} of dry nitrogen to avoid the oxidation induced degradation and to exclude the humidity effect.

For the case of the carbon/carbon composite, a non-contact type apparatus using He–Ne gas laser was utilized for the CTE measurements in the temperature range of room temperature to 2000°C. The sample dimensions of the carbon/carbon composite were $3 \times 5 \times 40$ mm. The measurements were carried out under 2°C min^{-1} of temperature increase rate and Ar atmosphere.

5. Discussion

Here we will re-examine the previous data reported by other researchers and the experimental data, which we generated in the present study by comparing them with the present models.

5.1. Mechanisms of reduction in composite CTE due to voids

We first attempt to provide a mechanism of the reduction in the composite CTE due to voids. Let us pay attention to the thermal stress field in a particulate (spherical particle) composite, where the CTE and elastic modulus of the reinforcement are assumed to be lower and higher than those of matrix resin, respectively. When this composite is subjected to temperature rise ($\Delta T > 0$), CTE mismatch strain ($= \Delta T(\alpha_f - \alpha_m)$) is induced. This CTE mismatch strain gives rise to compressive and tensile stress fields in the matrix and particles, respectively. If microvoids are dispersed in the matrix, the microvoids are subjected to the compressive stresses, resulting in the shrinkage of the void volume. Hence, the overall CTE of the composite is reduced. This is a fundamental mechanism by which we can explain the thermal expansion behavior already demonstrated. The induced thermal stresses are higher for a

fiber composite system than for a spherical composite system. If disk-shaped (penny-shaped) voids are mixed with the matrix, the voids are compressed more easily than the spherical voids. Thus, according to the void compression mechanism, we can expect more drastic effect of disk-shaped voids on the CTE of the fiber composite.

Another mechanism that can contribute to the CTE reduction is the decrease in volume fraction of the matrix material in the composite. By mixing voids in the matrix, the net volume fraction of the matrix decreases with increase of the amount of the void volume fraction. Hence, the influence of the matrix, which has a large CTE is reduced with increase of volume fraction of voids, contributing to the CTE reduction. This second mechanism, however, can be considered a minor source of the CTE reduction because it can not explain the large amount of CTE reduction demonstrated in the following numerical and experimental results. Thus, the void compression mechanism plays a key role to reduce composite CTE.

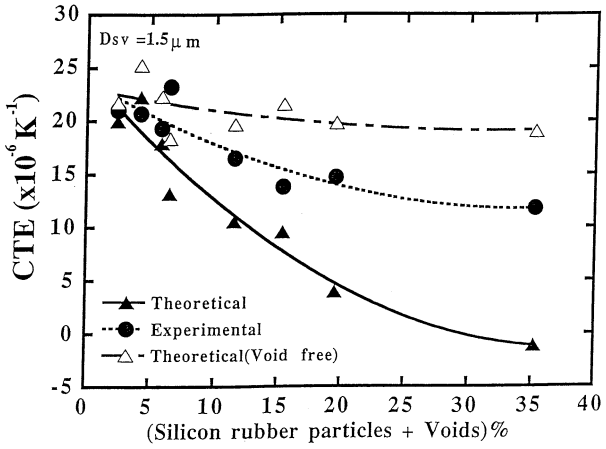

Fig. 15. In-plane CTE of a short fiber composite as a function of void volume fraction V_v.

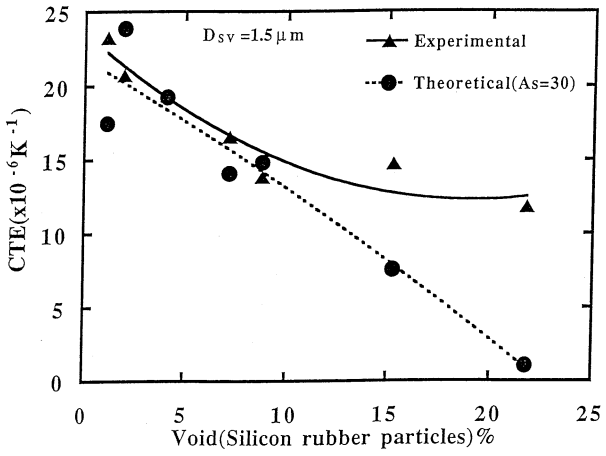

Fig. 16. In-plane CTE of a short fiber composite as a function of volume fraction of silicon rubber particles V_{vs}.

5.2. Short fiber reinforced composite

The CTEs of the void-dispersed short fiber composite along the in-plane direction are shown as a function of volume fraction of voids V_v, in Fig. 15, where the volume fraction of the silicon rubber V_{vs} is varied from 0 to 20. However, unexpected voids with volume fraction V_{vp} were inevitably introduced during forming process of composites. The horizontal axis in Fig. 15 thus denotes the sum of V_{vs}, and V_{vp}. In this figure ▲, ●, and △, represent theoretically predicted and experimentally observed CTEs and CTE for void-free composite with the same V_f as in the case of ●, respectively. Though there exists scattering of data even in the predicted values due to the variation of V_f in these composites, it is obvious from the figures that the theoretical model (including voids) predicts lower values than the experimental CTEs. On the contrary, the experimental values are in an agreement with theoretical predictions, if the only V_{vs} (the volume fraction of converted voids, which is in turn equal to that of silicon rubbers) is regarded as effective voids as shown in Fig. 16. Thus, it is obvious that only V_{vs} contributes to lowering the composite CTE. The reason for this behavior can be understood by examining SEM photos of Al_2O_3 short fiber composite (Fig. 17) where a and b correspond to the case of larger and smaller volume fraction of voids, V_v. Namely, when V_v, becomes high, the percentage of the volume fraction of process-inducted voids (V_{vp}) in V_v, becomes high. Many of the voids introduced in the forming process have by itself a huge volume compared with that of the silicon rubber particles and the Al_2O_3 short fiber as shown in Fig. 17. The void effect in reducing the composite CTE occurs by the compressive stress field developed just around the reinforcements as mentioned earlier. Hence, the void effect is most effective only if the size of voids is about the same as or smaller than the reinforcement. This is the reason why the voids made by the silicon rubber particles are effective but the process-induced voids whose size is larger than that of the converted voids from silicon rubbers are ineffective in reducing the composite CTE.

It should be noted in Fig. 16 that the experimentally obtained CTEs tend to deviate from the theoretical predictions when V_{vs}, becomes higher than 10%. The reason for this deviation is that at higher volume fraction of voids more process-induced voids are formed in the composite, resulting in less effectiveness of reducing the composite CTE.

5.3. 3D composites

Fig. 18 shows the relation between the CTEs of tri-axial 3D composite and the void volume fraction V_v. It should be noted in the figure that, in the region of

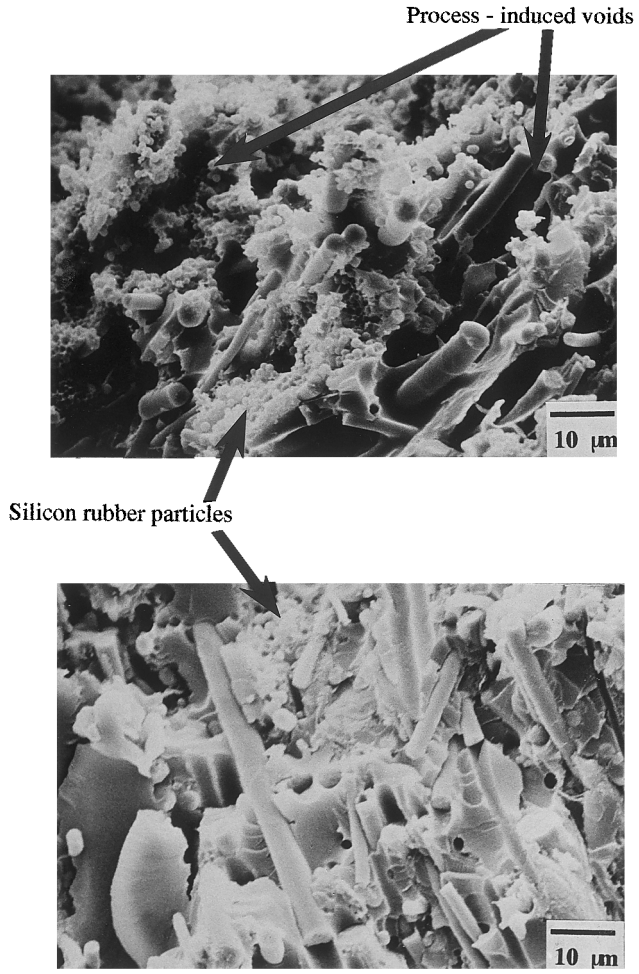

Fig. 17. SEM microphotograph of fraction surfaces for short fiber composites when $V_v = 35.2\%$, $V = 21.8\%$ (a) and $V_v = 11.5\%$, $V = 20.5\%$ (b).

$V_v < 10\%$, CTE decreases rapidly with increase of V_v and this behavior is predicted reasonably well by the void dispersion model, (Fig. 4b). On the other hand, CTE takes on an almost saturated value of $1-2 \times 10^{-6}$ in the region of $V_v > 10\%$. The void dispersion model is not adequate in this region but the thinly coated model (Fig. 4a) predicts reasonably well though the observed values are slightly higher than the predicted ones.

5.4. Laminated carbon/carbon composites

In Fig. 19 experimentally obtained in-plane CTE of the laminated carbon/carbon composite with quasi-isotropic stacking sequence is compared with that of the theoretical predictions. Both crackless and transverse cracks (TCs) cases were calculated to simulate CTF behavior of the laminated carbon/carbon composite. The average of the aspect ratio (2D) of TCs in the carbon/carbon composite was about 15–20 and volume fraction, V_{TC}, was 3%. Thus in the calculation disk-shaped void having aspect ratio $A_{TC} = 1/20$ were assumed to be dispersed in the matrix for the simulation of the TCs-dispersed laminated carbon/carbon composite. Details of microstructure and CTE behavior of this composite are shown in recent paper [9]. It is obvious from this figure that the prediction agrees well with the experimentally observed in plane CTE. As for the CTE along the out-of-plane direction, the effect of the TCs was negligible and this tendency also coincides with the theoretical prediction by the present model. The similar results were obtained for the laminated carbon/carbon composite with the cross ply (0, 90°) stacking sequence [18].

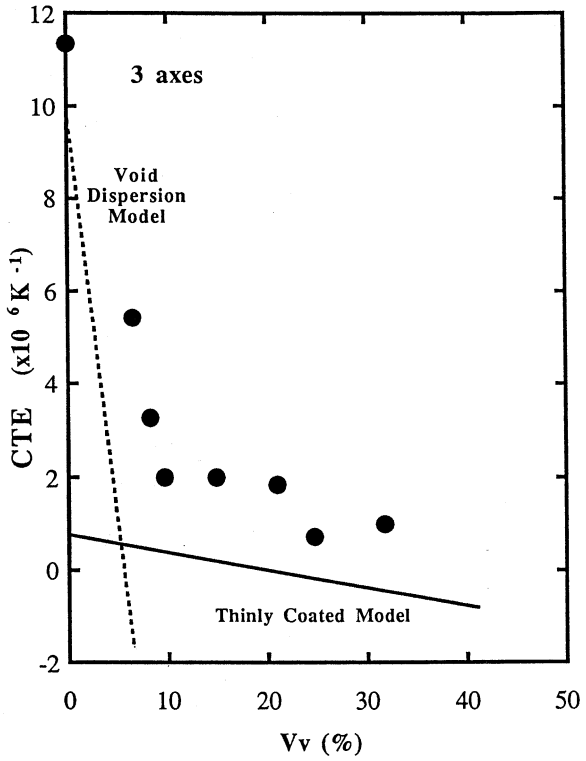

Fig. 18. Relation between thermal expansion coefficient CTE and volume fraction of voids V_v, for tri-axial skeletonized composites.

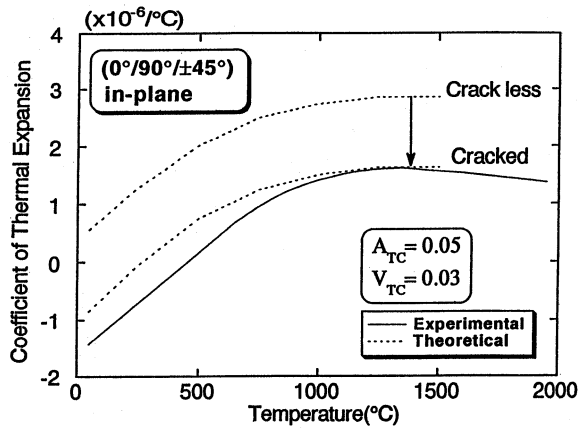

Fig. 19. Temperature dependence CTE of the quasi-isotropically laminated (0, 45, 90, −45°) carbon/carbon composite.

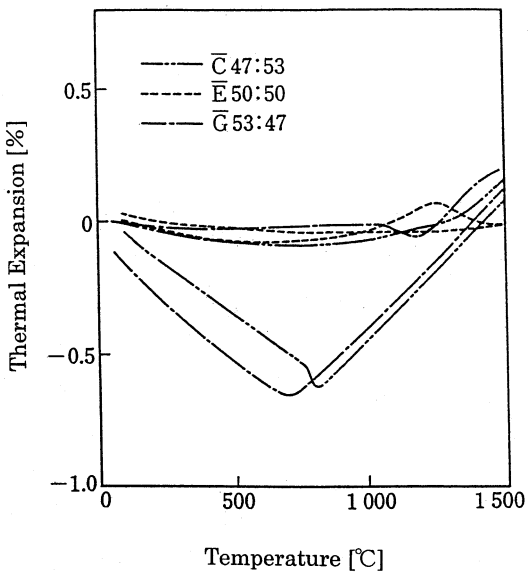

Fig. 20. Temperature dependence of thermal expansion in Al_2O_3/TiO_2 composite, after Hirono et al. [20].

5.5. Limitation of the void effect on CTE

As demonstrated in the above data, there seems to be some upper limit on the volume fraction of voids (V_v) up to which the composite CTE can be effectively reduced by dispersing voids in the matrix. This upper limit is expected to be dependent upon the type of reinforcement. For example, for the particulate composite, there exists no limit while in a short fiber composite the upper limit is about 10%. This limit of V_v in the short fiber composite is due to the difficulty inherent in processing of the composite with high volume fraction of silicon rubber particles without introducing processing-induced voids.

For a 3D composite this limit appears to be about 10%. This limit may be induced by high magnitude of internal stresses. In a 3D composite, high value of thermal stresses must be induced at the interface between the reinforcement and matrix due to large CTE mismatch. It is shown that higher magnitude of thermal stress tends to be induced in 3D composite compared with the 1D (aligned) or 2D (laminate) composites [15]. If the interface is strongly bonded then a large amount of the composite CTE reduction can be predicted. It is more likely however, that these high values of thermal stresses give rise to fracture at the interface. Thus, in this respect the compressive thermal stress, which is the main driving force of the composite CTE reduction effect by voids, is relaxed by the existence of the interfacial cracks. Then the void effect in reducing the composite CTE is diminished. Thus, the above mechanism can explain the upper limit of the volume fraction of voids in effectively reducing the composite CTE.

The results in this study suggest that lower limit of CTE by the void effect appears to be that of reinforcement, i.e. silica, alumina CFRP rod, and carbon fiber for the composites examined in this study. However, larger amount of CTE reduction can be further expected by combination, e.g. fiber-shape reinforcement and appropriately dispersed disk-shape voids, and we can possibly design a composite with negative value of CTE even if the CTEs of the constituent materials are positive. For the case of low CTE ceramics, e.g. Al_2O_3–TiO_2, negative CTE is actually obtained even though the CTEs of constituents are positive as reported by Hamano et al. [20] (see Fig. 20). The negative CTE of this Al_2O_3–TiO_2 is said to be brought by incorporation of microcracks in the grain boundary, strong anisotropic CTE of the constituent material, and thermal loading. The negative CTE of this case can possibly be predicted by the present model with minor modification.

6. Concluding remarks

It was found in this study that a large amount of CTE reduction can be achieved by dispersing voids in the matrix and this effect is induced by the compressive thermal stress in the matrix due to CTE mismatch of constituents. Experimental verification of this analytical model was also made for four kinds of composite systems dispersed micro-voids. It is confirmed from the comparison that a large amount of CTE reduction as predicted by our analytical model can be actually obtained by dispersing voids in various composite materials. However, the region of V_v in which this mechanism acts effective, is restricted for several reasons. For the particulate composite we could not find this limit and for the short fiber and 3D composites the limits of V_v were 10 and 6–7%, respectively.

References

[1] T. Takei, H. Hatta, M. Taya, Mater. Sci. Eng. A131 (1991) 133.
[2] T. Takei, H. Hatta, M. Taya, Mater. Sci. Eng. A131 (1991) 145.
[3] A. Noda, T. Fujimoto, S. Kita, Y. Yamamoto, Preprint of 60th Annual Meeting of the Chem. Soc. Jpn., 1990, 4C325.
[4] J.D. Eshelby, Proc. R. Soc. London A241 (1957) 376.
[5] D.K. Hale, J. Mater. Sci. 11 (1976) 2105.
[6] G.J. Dvorak, J. Appl. Mech. 53 (1986) 737.
[7] K. Wakashima, M. Otsuka, S. Umekawa, J. Compos. Mater. 8 (1974) 391.
[8] G.J. Dvorak, T. Chen, J. Appl. Mech. 56 (1986) 418.
[9] K. Schulgasser, J. Appl. Mech. 56 (1989) 546.
[10] K. Takahashi, K. Harakawa, T. Sakai, J. Compos. Mater. Suppl. 14 (1980) 144.
[11] Y. Takao, in: J.R. Vinson, N.L. Taya (Eds.), Recent Advances in Composites in the United States and Japan, ASTM STP 864 (1985) 685.

[12] Y. Takao, T. Taya, J. Appl. Mech. 52 (1985) 806.
[13] T. Takei, H. Hatta, T. Ishikawa, Mater. Sci. Eng. A161 (1992) 213.
[14] H. Hatta, J. Jpn. Soc. Compos. Mater. 14 (1988) 73.
[15] H. Hatta, T. Takei, M. Mori, Zairyo System 10 (1991) 71.
[16] T. Chou, T. Nakagawa, A. Okura, Todai-Seiken Houkoku 35 (1991) 1.
[17] E. Yasuda, Y. Tanabe, H. Machino, A. Takaku, Proc. 13th Bienn. Conf. Carbon, 1987, p. 30.
[18] Y. Saito, S. Nomura, H. Imai, Tanso 146 (1991) 22.
[19] H. Hatta, Y. Kogo, Y. Yoshihara, Y. Sawad, K. Takahashi, K. Hosono, T. Dozono, Zairyo System 14 (1995) 15.
[20] T. Hamano, Proc. 29th Fall Meeting Jpn. Soc. Chem, vol. 1, 1978, p. 542.